Tidal Motion in Submarine Canyons—A Laboratory Experiment

PETER G. BAINES

CSIRO Division of Atmospheric Physics, Aspendale, Australia

ABSTRACT

The reasons for the large-amplitude tidal motion observed in oceanic submarine canyons have been explored with a laboratory experiment. A barotropic tide was forced in a stratified tank, containing continental shelf-slope topography into which a narrow canyon was incised. Large-amplitude tidal motions were observed in the canyon; it is shown that these were forced by the large horizontal pressure gradient existing on the continental shelf near the canyon head. Another significant feature of this experiment was that internal waves inside the canyon were partially reflected from the open boundary at the mouth of the canyon, like sound waves from the open end of an organ pipe. This enabled energy to propagate down the canyon in the form of leaky modes.

The character of the flow in the canyon was strongly dependent on the ratio of bottom slope α to ray (or characteristic) slope c. For $\alpha/c \ll 1$ the stratification had little effect on the motion, and the largest displacements were nearly barotropic and occurred near the canyon head; for $\alpha/c \approx 1$ the motion was baroclinic and had the same pattern at all depths. For $\alpha/c > 1$ the energy propagated down the canyon in the form of leaky modes; because of reflection at the bottom, large amplitudes may occur near there in some cases.

The analysis also suggests a mechanism for the large amplitudes of high-frequency internal waves observed in submarine canyons. For a narrow canyon, wave motion in the canyon will be forced at the mouth by the pressure field of an incident wave from the deep sea, plus that of the wave reflected from the external continental slope; this will result in a wave with up to twice the amplitude (and hence four times the energy) inside the canyon.

1. Introduction

Observations of currents in submarine canyons indicate that, rather than being quiet backwaters, they are dynamically very active regions on a broad band of time scales, ranging from upwelling and turbidity-current phenomena to tidal and higher internal-wave frequencies. The book by Shepard *et al.* (1979) describes observations made in a substantial number of canyons distributed around the world, and the ubiquity of the large tidal velocities (in particular) is striking. Wunsch and Webb (1979) have demonstrated that internal-wave energy levels inside Hydrographer Canyon (off the U.S. east coast) are quite large over a broad range of frequencies. The most extensive study to date is in Hudson Canyon (Hotchkiss, 1980; Hotchkiss and Wunsch, 1982); at a number of locations distributed throughout the canyon, tidal and internal-wave velocities were high, and the tidal velocities increased as one moved up the canyon toward the head.

In view of the general character of the above observations it was decided to carry out a laboratory experiment to test the hypothesis that the large-amplitude tidal velocities (at least) were due to the three-dimensional nature of the canyon geometry. The experiment consisted of a finite tank filled with stratified fluid in which an oscillatory barotropic motion was generated at one end, and a continental shelf/slope geometry with a narrow incised canyon was placed at the other. As is found in the ocean, substantially larger displacements were observed in the canyon than on the continental slope outside the canyon, at the same depths. The spatial structure of this motion varied substantially with the ratio α/c, where α is the bottom slope (the same in the canyon as on the continental slope) and c is the slope of the rays for internal waves at the tidal (forced) frequency. In order to interpret these observations we employ the internal-tide generation theory, of which a complete description is given by Baines (1982). For a sufficiently narrow canyon we may make the assumptions that the presence of the canyon has negligible effect on the motions external to it and that the motion inside the canyon is driven by the external pressure field at its open boundaries. As is shown below, this approach gives a satisfactory description of the motions in the experiment.

The plan of the paper is as follows. The nature and details of the experiment are described in Section 2, together with some examples of the observations. Sections 3, 4 and 5 then develop the theory required for the interpretation of these observations. The nature of the motion of a fluid which is not stratified

is described in Section 3, in the linear low-frequency limit, for flow both inside and outside the canyon. Section 4 gives the equations for the stratified flow outside the canyon and Section 5 the corresponding motion inside the canyon. A quantitative comparison between the theoretical descriptions and the observations is given in Section 6, where the changing character of the flow with α/c is described in detail. The conclusions are summarized in Section 7.

One novel feature of this work is the recognition that internal waves may reflect from an open boundary (in this case, the canyon mouth) in much the same way as sound waves reflect from the open end of an organ pipe. As the gap width tends to zero the incident wave energy becomes totally reflected, but with a phase difference of 180° from that which is reflected from a rigid boundary. This phase change produces some interesting effects which may result in large amplitudes near the foot of the canyon. The complete diffraction problem for an internal wave in a slit incident on a half-space is solved elsewhere (Grimshaw et al., 1982), but the reflection coefficients as a function of the gap (or canyon) width are given here for the topographic slope of the experiment ($\alpha = 0.649$).

Care is required in applying the results of this paper to the ocean for two main reasons. First, the experiment is non-rotating; the presence of rotation would result in further complications in the form of internal Kelvin waves and associated cross-canyon variations, although the same general dependence of the flow character on α/c is expected. Second, the theory and experiment are appropriate to canyons of approximately uniform horizontal cross-section and width. The properties of real canyons with V-shaped cross-sections and wide mouths may be significantly different.

2. Description of apparatus and experiment

Most of the experiments were carried out with a transparent tank 22.9 cm wide and 183 cm long, and the configuration is illustrated in Fig. 1. Two-dimensional continental shelf/slope topography was inserted at one end of the tank. The "continental shelf" consisted of a horizontal surface 30.8 cm above the tank floor, spanning the width of the tank and extending from one end with a length of 45.0 cm. The plane "continental slope" section sloped downwards from the edge of the shelf (the "shelf-break") at an angle of 33° to the tank floor. Both the shelf and slope sections were made of polystyrene. A narrow slit (constituting the "canyon") was cut into this two-dimensional topography adjacent to a tank side wall. The horizontal length of this slit was constant with height and measured 16.7 cm in from the slope, so that the canyon floor had the same 33° slope as the continental slope. Initially, the canyon was tapered
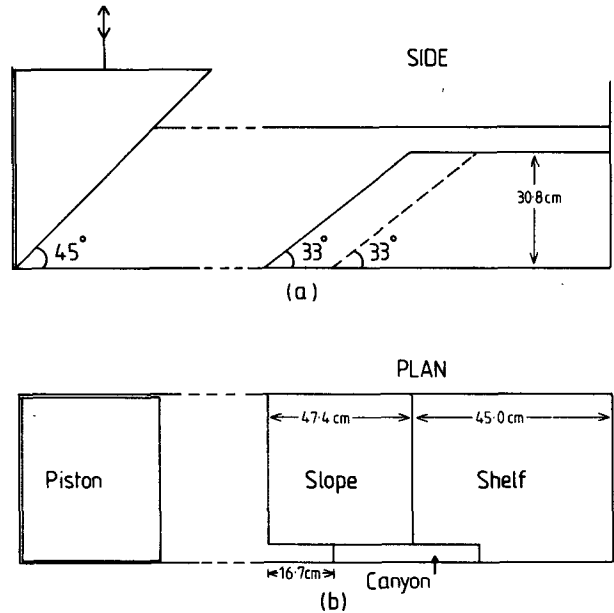

FIG. 1. Diagrams (not to scale) showing the side (a) and plan (b) views of the tank.

very slightly outwards, being 2.5 cm wide at the floor and widening to 3.5 cm at the mouth. Several quantitative runs were made with this narrow slope. Later the canyon was widened near the foot so that it narrowed in both the horizontal and vertical as one moved inwards from the foot toward the head. These two shapes are shown in Figs. 2a and 2b, respectively.
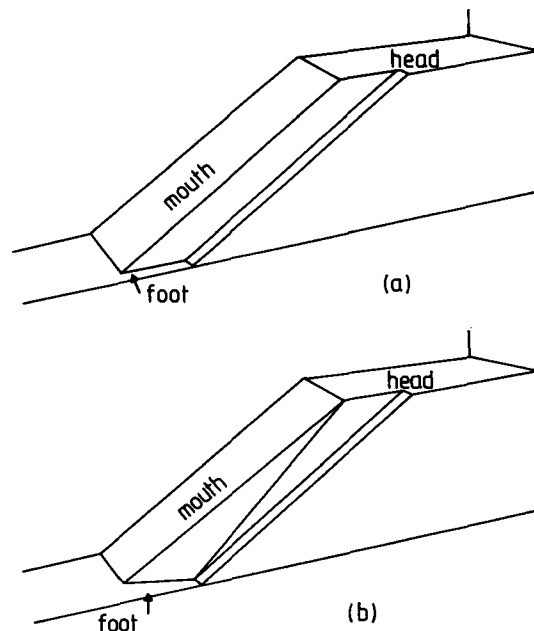

FIG. 2. The two canyon geometries used in the experiments: (a) narrow canyon, Runs 10–14; (b) wider canyon at the foot, Runs 15–18 (see Table 1).

At the other end of the tank a large solid wooden isosceles-triangular piston (angles 90°–45°–45°) was inserted. This spanned the tank width and was oriented with one short face against the end wall and a 45° vertex pointing downwards reaching almost to the bottom (See Fig. 1). The gap between the piston and the side and end walls was approximately 2 mm. This piston was connected to an electric motor, which enabled it to be oscillated vertically over a range of amplitudes and frequencies.

The tank was filled with a stratified fluid to a depth h_m of ~ 35 cm (~ 4.5 cm above the continental shelf) using the common two-tank method; in a tank with vertical side–walls this would have produced stratification with a constant density gradient. However, because of the changing cross-sectional area with height, the density gradient was not quite constant, but increased slightly with height up to the continental shelf level. During the filling process, potassium permanganate was injected at regular intervals into the filling hose near the inlet, and this resulted in horizontal dyed layers in the tank. With careful injection these layers were initially quite sharp but they thickened within a few hours on account of molecular diffusion. They formed the main means of flow visualization used in the experiment.

The experimental procedure was as follows. The motor which oscillated the piston was turned on; after a time interval of 5 minutes or longer to allow the system to reach a periodic state, photographs were taken at various phases of the piston from the side view, recording the displacements of the dyed layers both in the canyon and over the slope. Several runs were also recorded on movie film.

The experiments as described above were performed at the Woods Hole Oceanographic Institution; subsequent experiments with the same canyon geometry but a longer tank (220 cm) and shelf length (63 cm) were performed later at Aspendale to verify various aspects of the interpretation. One of these runs is described here (Run 1A, Fig. 5).

The piston motion resulted in a low-frequency oscillation in the free surface displacement in the tank. This motion is described in detail in the next section. The 45°-triangular piston was chosen to eliminate the direct generation of any baroclinic motion by the piston. During operation, some small-scale baroclinic motion was visible near the bottom vertex and near
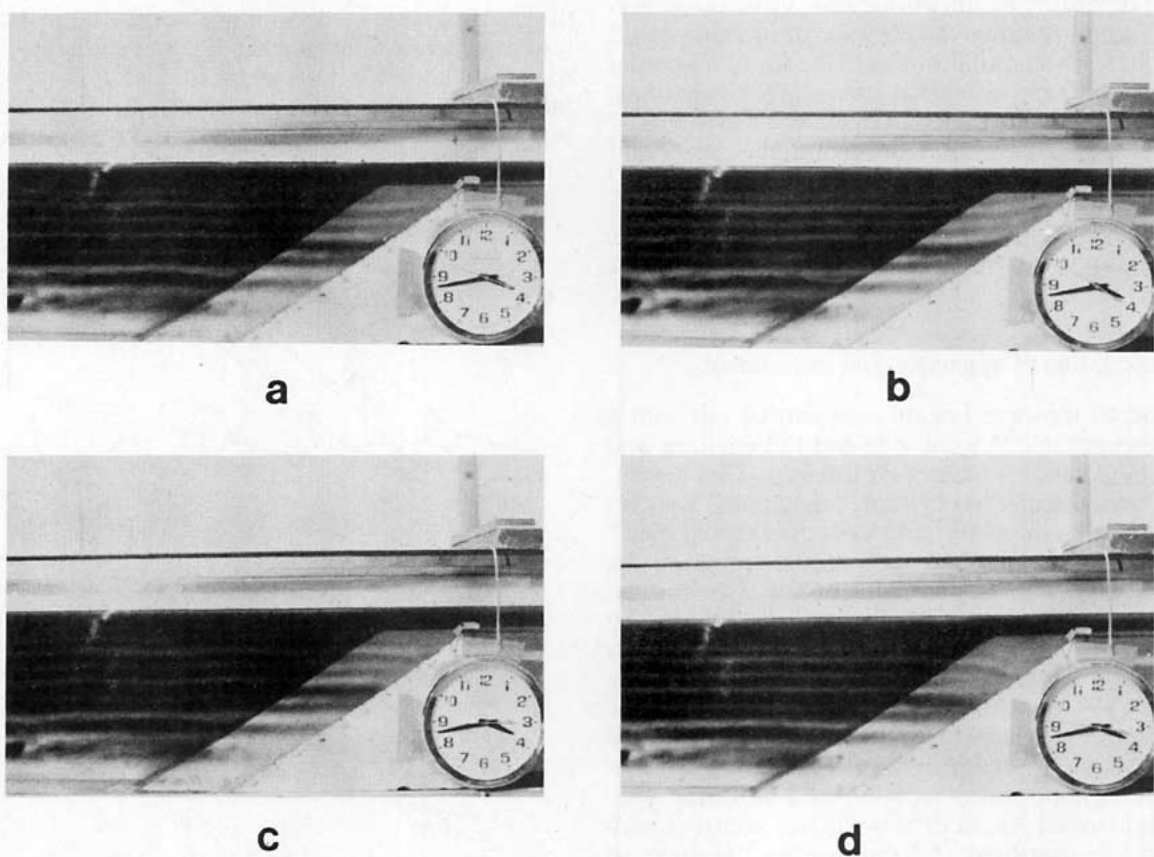

FIG. 3. Photographs taken at the four main phases of the tide for $\alpha/c = 0.25$ (Run 13); (a) maximum flood tide; (b) high tide; (c) maximum ebb; (d) low tide.

the intersection of the piston with the free surface, but this had very small amplitude and was inconsequential.

The forced horizontal fluid motion over the sloping topography resulted in the generation of internal-wave motion of the same frequency (internal tides). Over the two-dimensional slope these waves tended to propagate away from the generation region, which was concentrated near the shelf break. No baroclinic motion was visible over the shallow continental shelf, where some weak but persistent mixing due to bottom stress was apparent. The waves on the deep-water side propagated toward the piston end. Generally speaking these were small-scale waves in terms of the tank dimensions, and would be severely attenuated by viscosity whilst propagating from the shelf break region to the piston and back. No significant reflected waves could be observed during the experiment, and theoretical estimates of the wave dissipation (Appendix B) indicated that the reflected waves were negligible in the flow areas of interest (i.e. mainly in the canyon). Inside the canyon the observed motion was very nearly two-dimensional, except for the wider canyon (Figure 2b) near the mouth where some cross-canyon variation was apparent. The presence of the tank side-

wall had no visible effect on the motion of the dyed layers. For oscillatory motion with frequency ω we expect a Stokes boundary layer of thickness $(\nu/\omega)^{1/2}$ where ν is the kinematic viscosity, giving a thickness of O(1 mm) in these experiments, which is negligible.

Some representative observations of the flow in the canyon and over the slope are shown in Figs. 3–5. The prinicipal dimensionless parameter governing the character of the flow is α/c, where α is bottom slope and $c = \omega/(N^2 - \omega^2)^{1/2}$, the internal-wave ray slope. In Fig. 3 the flow is representative of cases where $\alpha/c \ll 1$ (here specifically $\alpha/c = 0.25$, Run 13, Table 1), with the motion in phase with the piston motion and with large displacements concentrated near the head of the canyon. In Fig. 4 the flow is representative of $\alpha/c \approx 1$ (specifically $\alpha/c = 1.0$, Run 17); the flow in the canyon generally has the same amplitude and phase at all depths, and the motion is no longer in phase with the piston motion. In Fig. 5, where α/c is somewhat larger than unity (specifically $\alpha/c = 1.69$, Run 1A), the motion in the canyon is again large and is conspicuously baroclinic.

It is obvious from these observations that the three-dimensional canyon geometry results in large-amplitude tidal motions in the canyon, particularly when
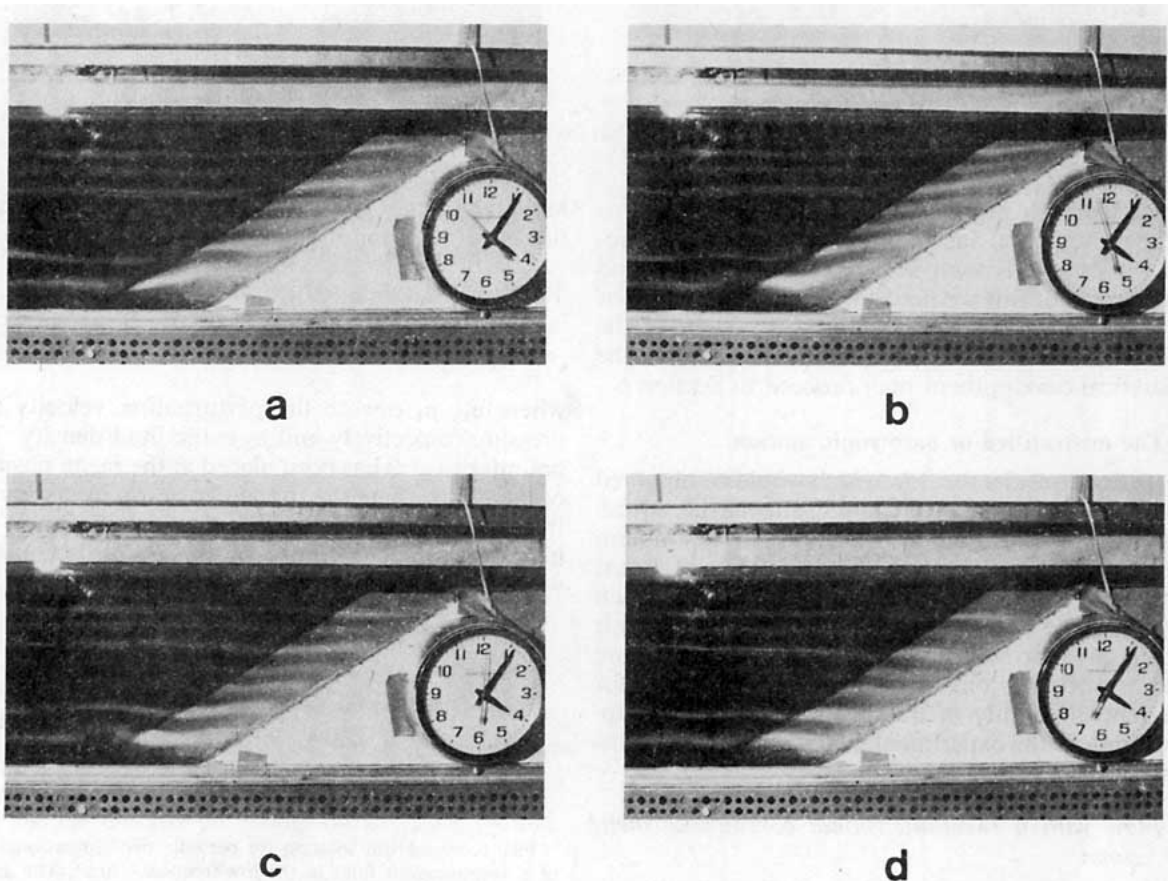

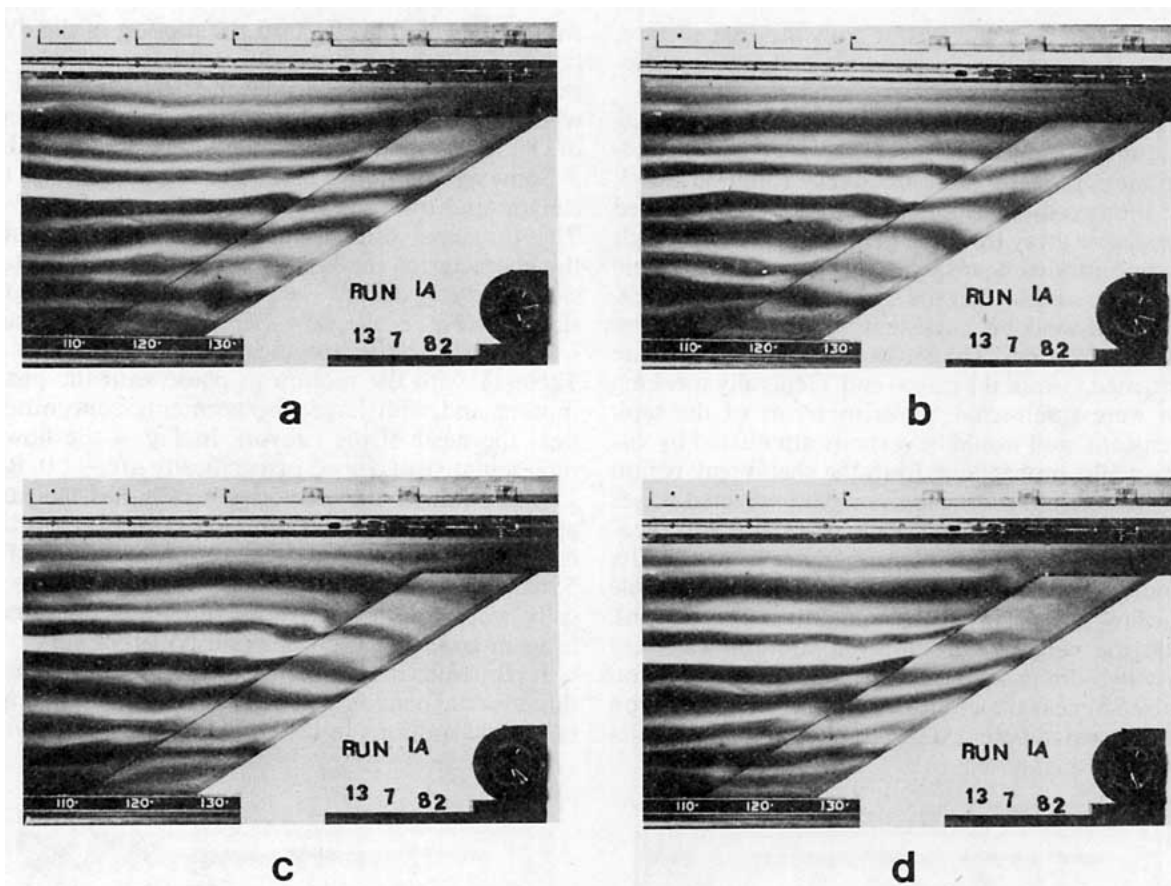FIG. 4. As in Fig. 3 but for $\alpha/c = 1.0$ (Run 17).

FIG. 5. As in Fig. 3, but for $\alpha/c = 1.69$ (Run 11).

contrasted with motions over the continental slope at the same depth, and that the character of this motion varies greatly with α/c. In order to understand the reasons for this we need to construct a theory for wave motion in the canyon, and this is done in the next three sections. Readers who wish to omit the theoretical development may proceed to Section 6.

3. The unstratified or barotropic motion

We first consider the flow which would be observed in the tank if the water were homogeneous (i.e. a fresh water fill). This is done in two stages: we first obtain the flow in the tank with the canyon assumed absent so that the topography is two-dimensional, and then we obtain the flow in the canyon assuming that it is sufficiently narrow to have little effect on the pressure field immediately outside it. Conditions required for the general validity of this assumption, and its applicability to the experimental configuration, are discussed below.

a. Flow with a two-dimensional continental shelf/slope

We consider a configuration as shown in Fig. 6, which gives a representation of the side view of the

tank and defines the quantities involved. In the usual notation the equations governing the fluid motion are

$$\left. \begin{array}{c} \mathbf{u}_{1t} + \mathbf{u}_1 \cdot \nabla \mathbf{u}_1 = -\dfrac{1}{\rho_0} \nabla p_1 \\[2mm] \nabla \cdot \mathbf{u}_1 = 0 \end{array} \right\}, \qquad (3.1)$$

where $\mathbf{u}_1$, p_1 denote the perturbation velocity and pressure respectively and ρ_0 is the fluid density. The boundary $x = 0$ has been placed at the mean position of the point where the triangular piston intersects the free surface, and we assume that at this point the horizontal velocity forced by the piston is constant with depth. The boundary condition is then
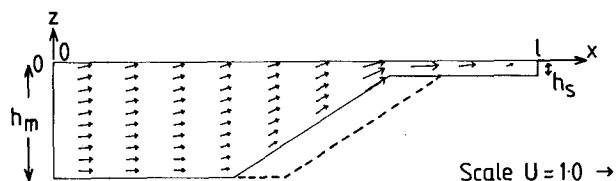

FIG. 6. Numerical solution for periodic two-dimensional flow of a homogeneous fluid in the low-frequency limit. The arrows give velocity vectors at peak flood tide. The dashed region shows the location of the canyon in Fig. 7.

$$u_1 = u_p \cos\omega t = \text{Re}[u_p e^{-i\omega t}], \quad x = 0, \quad (3.2)$$

and since the piston face is at an angle of 45° to the horizontal we have

$$u_p = \omega a_p,$$

where a_p is the (small) vertical amplitude of the piston motion. The other boundaries are rigid apart from the free surface, which oscillates vertically with an amplitude $a_p h_m/l$ in the mean, where h_m is the fluid depth in the deepest region, and l is the effective length of the tank (i.e. total length minus piston length at surface).

We scale the above equations formally by writing

$$\left.\begin{array}{l} X = x/h_m, \quad Z = z/h_m \\[4pt] T = \omega t, \quad H(x) = h(x)/h_m \\[4pt] U = u_1/u_p, \quad W = w_1/u_p, \quad P = ip/\rho_0\omega u_p h_m \end{array}\right\} . \quad (3.3)$$

We thus obtain

$$\left.\begin{array}{l} U_T + \dfrac{a_p}{h_m}(UU_X + WU_Z) = iP_X \\[10pt] W_T + \dfrac{a_p}{h_m}(UW_X + WW_Z) = iP_Z \end{array}\right\}, \quad (3.4)$$

with the boundary conditions

$$\left.\begin{array}{llll} U = \text{Re}[e^{-iT}], & \text{at} & X = 0 \\[4pt] \mathbf{U}\cdot\hat{\mathbf{n}} = 0, & \text{at} & Z = -H(X) \\[4pt] & \text{and} & X = 1/\beta = l/h_m \end{array}\right\} \quad (3.5)$$

together with the free surface condition. This scaling does not consider the variable depth or shallow topography, but it is clear that if a_p and ω are sufficiently small, and if resonances in the tank are avoided, the nonlinear terms will be negligible and the motion will have harmonic time dependence. The free surface condition in linearized form then may be written

$$P_Z = \omega^2 h_m g^{-1} P - \beta e^{-iT}, \quad (3.6)$$

where the real part is taken.

If we regard the time dependence as implicit and with $\omega^2 h_m/g \ll 1$ the equations are

$$\left.\begin{array}{l} U = -P_X, \quad W = -P_Z \\[4pt] U_X + W_Z = 0 \end{array}\right\}, \quad (3.7)$$

with

$$\left.\begin{array}{llll} U = 1, & \text{at} & X = 0 \\[4pt] \nabla P \cdot \hat{\mathbf{n}} = 0, & \text{at} & Z = -H(X) \\[4pt] & \text{and} & X = 1/\beta \\[4pt] P_Z = -\beta, & \text{at} & Z = 0 \end{array}\right\}, \quad (3.8)$$

so that we require the solution of Laplace's equation. These equations describe the motion in the tank in the low frequency limit.

In the experiments the parameter values were

$$\left.\begin{array}{l} a_p \leqslant 1.9 \text{ cm}, \quad h_m = 35.5 \text{ cm} \\[4pt] l = 147.5 \text{ cm}, \quad \omega \leqslant 0.83 \text{ rad s}^{-1}, \quad \text{so that} \\[4pt] a_p/h_m \leqslant 0.05, \quad \omega^2 h_m g^{-1} \leqslant 0.02 \end{array}\right\} . \quad (3.9)$$

Eqs. 3.7, 3.8 have been solved numerically using a standard package (IMSL TWODEPEP) which employs a finite element method, and the associated velocity field is displayed in Fig. 6.

We next discuss an analytic approximation to the flow over the slope which illustrates its character and is useful in describing it. We begin by assuming that the flow is hydrostatic, so that U is essentially independent of depth. This is a good approximation in the ocean where $\alpha \ll 1$, but is not so appropriate in the tank where $\alpha \approx 0.65$; nonetheless, it gives a reasonable description of the gross properties of the flow field.

We therefore assume that U is independent of Z, and integrating the continuity equation (3.7) with respect to depth gives

$$\frac{d}{dX}(HU_1) = -\beta, \quad (3.10)$$

where the suffix "1" denotes the hydrostatic solution. Integrating and using the boundary conditions then gives

$$U_1(X) = \frac{1 - \beta X}{H(X)}, \quad 0 < X < 1/\beta. \quad (3.11)$$

According to this expression, the fluid velocity decreases linearly away from the piston above the horizontal bottom, increases with X on account of decreasing depth over the slope, and then decreases linearly to zero over the shelf; the largest fluid velocity occurs over the shelf break. From U_1 we may obtain a corresponding W_1 from the continuity equation, namely

$$W_1 = \beta - Z\frac{d}{dX}\left(\frac{1 - \beta X}{H}\right). \quad (3.12)$$

U_1, W_1 satisfy all the equations and boundary conditions (3.6), (3.7), except for the equation $W = -P_Z$ and the singular points at the top and bottom of the slope.

In practice, in the tank the slope α is too large for the flow to be purely hydrostatic. For a region which has a constant slope α, we may construct a local power series solution in Z of the form

$$U, W, P = \sum_{n=1}^{\infty} (U_n, W_n, P_n), \quad (3.13)$$

where

$$U_n = -P_{nX}, \quad U_{nX} + W_{nZ} = 0, \quad W_n = -P_{n+1Z}, \quad (3.14)$$

with the hydrostatic solution constituting the first

term. Each successive term (U_n, W_n) satisfies the homogeneous boundary conditions at $Z = 0, -H$, and these together with the condition

$$\int_{-H}^{0} U_n dZ = 0, \qquad (3.15)$$

determine the constants of integration. The power series in Z generated by this procedure may be summed, after some algebra, to yield the solution

$$
\left.
\begin{aligned}
U &= \frac{1 - \beta X}{H} + \left[-\frac{\beta}{\alpha} + \frac{1 - \beta X}{H}\right] \\
&\quad \times \left[\frac{\alpha}{\arctan\alpha} \frac{1}{1 + (\alpha Z/H)^2} - 1\right] \\
W &= \beta - \frac{\alpha}{\arctan\alpha} \\
&\quad \times \left[-\frac{\beta}{\alpha} + \frac{1 - \beta X}{H}\right] \frac{\alpha Z/H}{1 + (\alpha Z/H)^2}
\end{aligned}
\right\} \quad (3.16)
$$

These expressions apply over a constant slope α, and in the limit $\alpha \to 0$ they reduce to U_1, W_1 for a horizontal bottom. Hence they describe the flow over the slope except for the effects of the corner points, and comparison with the numerical solution gives very good agreement in the range $67 < x < 95$ cm (the slope covers the range $55.1 < x < 102.5$ cm). In general, the horizontal velocity is increased at upper levels and decreased at lower levels, relative to the uniform hydrostatic profile.

b. Flow in the canyon

As shown in a simple model calculation in Appendix A, if

$$\frac{b_1}{B_1} \ll 1, \qquad \frac{\omega^2 b_1^2}{gh_s} \ll 1, \qquad (3.17)$$

where b_1, B_1 are the canyon and tank widths respectively and h_s is the depth on the shelf, then the presence of the canyon will have little effect on the true surface elevation and hence on the pressure and velocity field in the tank external to the canyon. In the experiment we have

$$\frac{b_1}{B_1} = 0.17, \qquad \frac{\omega^2 b^2}{gh_s} \lesssim 3.10^{-4}, \qquad (3.18)$$

so that the requirements are satisfied. From this we may assume that the "barotropic" motion inside the canyon will be driven by the pressure field set up just outside it by the two-dimensional flow field which would exist if the canyon were absent.

For a narrow canyon we may also assume that the motion in the canyon is two dimensional (it is generally observed to be so in the experiments—vide Figs. 3–5). The equations for the flow in the canyon are then (3.7), assuming linearity, with the boundary

conditions being the rigid boundary condition on the canyon floor and the imposed pressure field at the open boundaries. This problem has been solved numerically using the same procedure as described above for the external flow, and using the pressure field obtained on the slope and shelf from that calculation and given in Fig. 9. The resulting flow is shown in Fig. 7. Note that the largest velocities occur near the head of the canyon, and that the flow pattern is similar to that shown in Fig. 3 (as discussed in more detail below).

We may contrast this flow pattern with that which would be obtained if the flow were hydrostatic. In this case we would have in the canyon (in dimensional form),

$$\frac{\partial u_1}{\partial t} = -g\zeta_x, \qquad (3.19)$$

where ζ is the free surface elevation, and hence

$$u_1 \text{ (inside canyon)} = u_1 \text{ (outside canyon)}$$

for the same x value. Since u_1 is largest at the shelf break, this would give the largest horizontal displacements in the canyon at the point corresponding to the shelf break. However, in the tank, where the slope is too steep for the flow to be hydrostatic, the upslope velocities are found (in the numerical solution) to be independent of the coordinate normal to the bottom, rather than the vertical. Consequently, the largest velocities are found near the canyon head rather than directly beneath the shelf break. This simple mechanism for large amplitude motions near the upper regions of the canyon should have wide applicability in certain oceanic situations, as discussed below.

4. Baroclinic motion: theory for a two-dimensional tank

The linearized equations for a stratified two-dimensional fluid are
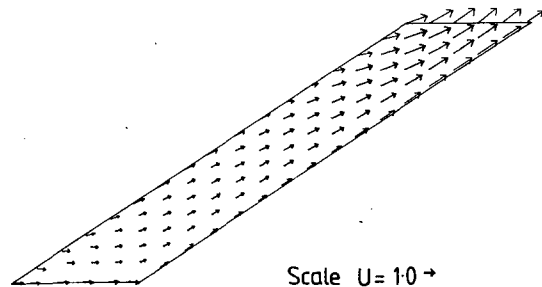

Scale $U = 1.0 \rightarrow$

FIG. 7. Numerical solution for two-dimensional flow of a homogeneous fluid in a narrow submarine canyon, forced by the external flow represented in Fig. 6. Arrows represent the velocity field at peak flood tide.

$$\rho_0 u_t = -p_x$$
$$\rho_0 w_t = -p_z - \rho g$$
$$\rho_t + w\rho_{0_z} = 0$$
$$u_x + w_z = 0$$
$$\left.\begin{array}{c}\\\\\\\\\end{array}\right\} , \quad (4.1)$$

where ρ_0 is the mean fluid density and ρ the perturbation.

We may express the total velocity and pressure fields in the form

$$\mathbf{u} = \mathbf{u}_1 + \mathbf{u}_i, \quad p = p_1 + p_i, \quad (4.2)$$

where $\mathbf{u}_1$, p_1 represent the motion with homogeneous water as described in the previous section; $\mathbf{u}_i$, p_i then represent the baroclinic flow. As in Section 3, we first discuss the two-dimensional motion exterior to the canyon, assuming that the latter is absent, and then discuss the motion in the canyon itself.

We again consider the region shown in Fig. 6. For two-dimensional motion we may define a stream function ψ by

$$u_i = -\psi_z, \quad w_i = \psi_x. \quad (4.3)$$

Substitution of (4.1), (4.2) into the equations of motion, linearized about a state of rest, and invoking the properties of $\mathbf{u}_1$ yields (e.g., Baines, 1973)

$$\nabla^2 \psi_{tt} + N^2(z)\psi_{xx} = -N^2 w_{1_x} = -N^2(z)\psi_{1_{xx}}, \quad (4.4)$$

where $N(z)$ is the Brunt-Väisälä frequency, ψ_1 is the corresponding stream function for $\mathbf{u}_1$ defined by

$$u_1 = -\psi_{1_z}, \quad w_1 = \psi_{1_x}, \quad (4.5)$$

and ψ satisfies the boundary condition

$$\psi = 0, \quad (4.6)$$

on all the boundaries.

With harmonic time dependence we may write

$$(\psi, \psi_1) = (\Psi, \Psi_1)e^{-i\omega t} \quad (4.7)$$

so that (4.3) becomes

$$\Psi_{xx} - c^2\Psi_{zz} = -(1 + c^2)\Psi_{1_{xx}}, \quad (4.8)$$

where

$$c^2 = \frac{\omega^2}{N^2(z) - \omega^2}. \quad (4.9)$$

To solve this equation we write

$$\Psi = \Psi_2 + \Psi_3, \quad (4.10)$$

where Ψ_2 is a particular solution of (4.8). A suitable particular solution is

$$\Psi_2 = -\Psi_1, \quad (4.11)$$

since Ψ_1 satisfies Laplace's equation. Ψ_3 then gives the *total* motion and satisfies

$$\Psi_{3_{xx}} - c^2\Psi_{3_{zz}} = 0, \quad (4.12)$$

with

$$\Psi_3 = \Psi_1 \quad (4.13)$$

on the boundaries. Hence the boundary conditions for Ψ_3 may be written

$$\Psi_3 = u_p h_m(x/l - 1), \quad z = 0$$
$$= 0, \quad z = -h(x)$$
$$= -u_p(z + h_m), \quad x = 0$$
$$= 0, \quad x = l$$
$$\left.\begin{array}{c}\\\\\\\\\end{array}\right\} . \quad (4.14)$$

We may write

$$\Psi_3 = u_p h_m(x/l - 1) + \Psi_3' \quad (4.15)$$

so that Ψ_3' also satisfies (4.12) but with

$$\Psi_3' = 0, \quad z = 0, \quad x = l$$
$$= u_p h_m(1 - x/l), \quad z = -h(x)$$
$$\left.\begin{array}{c}\\\\\end{array}\right\} . \quad (4.16)$$

Ψ_3 contains both barotropic and baroclinic motions, and the barotropic motions (in terms of the vertically integrated mass flux) are prescribed by the boundary conditions (4.13). Hence only the baroclinic structure is unknown. This baroclinic motion will be generated by the interaction of the barotropic tide with the topography, so that the problem is the same as the familiar internal-tide generation problem (e.g., Baines, 1973, 1974, 1982), provided that baroclinic wave reflection from the ends of the tank may be neglected. This may be justified under the conditions of the experiment, as shown below. We define the vertically integrated mass flux $Q(x)$ by

$$Q(x) = u_p h_m(1 - x/l). \quad (4.17)$$

When $\alpha/c < 1$ ("flat" topography), if $Q(x)$ and $N(z)$ are constant over the region of sloping topography the baroclinic motion $\Psi_i = \Psi_2 + \Psi_3$ will be small unless (Baines 1973)

$$\alpha/c > \frac{1 - h_s/h_m}{1 + h_s/h_m}. \quad (4.18)$$

In the present case with $h_s = 4.65$ cm, $h_m = 35.5$ cm, this requires

$$0.77 < \alpha/c < 1,$$

i.e., "single hop" geometry. In the experiments N is not constant in the lowest 10 cm, and Q varies by $\pm 30\%$ of its mean value over the slope. However, these variations appear to have little effect; the experiments with $\alpha/c < 1$ are all in the range $0 < \alpha/c < 0.84$, and the baroclinic motions over the slope are observed to be small compared with the barotropic motions. Their effects will be neglected in the interpretation of the motions in the canyon in the next section. For $\alpha/c < 1$, therefore, the pressure field on the topographic surface will be predominantly that

of the barotropic component, except where α/c is close to unity.

For $\alpha/c > 1$ the baroclinic motion is primarily generated near the shelf break, and the flow may be calculated with the assumption that the generation is local and the slope infinite in extent (Baines, 1982). If Q is constant and equal to Q_c (which in general denotes the value of Q at the shelf break $x = x_c$), then the velocity field over the slope may be written

$$
\begin{aligned}
u_3 = -\Psi_{3_z} = -\frac{Q_c}{4h_s} & \left[\begin{array}{ll} V\left(\frac{\eta}{2\gamma}\right) - V\left(-\frac{\xi}{2\gamma}\right), & \eta > 0 \\[2mm] -\frac{1}{q} V\left(1 - \frac{\eta}{2\gamma q}\right) - V\left(-\frac{\xi}{2\gamma}\right), & \eta < 0 \end{array} \right] \\[4mm]
w_3 = \Psi_{3_x} = -\frac{cQ_c}{4h_s} & \left[\begin{array}{ll} V\left(\frac{\eta}{2\gamma}\right) + V\left(-\frac{\xi}{2\gamma}\right), & \eta > 0 \\[2mm] -\frac{1}{q} V\left(1 - \frac{\eta}{2\gamma q}\right) + V\left(-\frac{\xi}{2\gamma}\right), & \eta < 0 \end{array} \right]
\end{aligned} \Bigg\} ,
\tag{4.19}
$$

where

$$
\left.
\begin{aligned}
\xi &= \int_0^z \frac{dz}{c} + x - x_c - \gamma \\[2mm]
\eta &= \int_0^z \frac{dz}{c} - (x - x_c - \gamma) \\[2mm]
q &= \frac{\alpha - c}{\alpha + c}, \quad \gamma = \int_{-h_s}^0 \frac{dz}{c}
\end{aligned}
\right\} .
\tag{4.20}
$$

The geometry is shown in Fig. 8, and the function V is given in Fig. 8 of Baines (1982). If Q is not constant these expressions are slightly more complicated but are still valid in the region $\eta < 0$ adjacent to the slope, although in general V will be slightly different. With regard to the effects of the ends of the tank, on the shallow shelf the motion described by this solution is essentially barotropic, and this is consistent with observations; hence the end at $x = l$ has no effect on the baroclinic motion. In the deep water, the structure of the relatively narrow beam is attenuated by viscosity. It is shown in Appendix B that, for the tank and parameters used in the experiment, baroclinic motion which is reflected from the generating piston will have greatly decreased amplitude when it reaches the topography. This is consistent with experimental observations: although some small-amplitude internal-wave motion could be observed in the deep water, no evidence of any coherent motion reflected from the deep end could be discerned near the topography.

Our primary objective in this study is the nature of the motion inside the canyon, which we regard as being forced by the pressure field at its open boundaries. Hence, we next calculate the pressure field on the surface of the two-dimensional topography. In (4.1) for the total flow, over the slope we may identify u, w with u_3, w_3, and, expressing these in terms of the pressure, we obtain

$$
u_3 = -\left(\frac{ip}{\rho_0 \omega}\right)_x, \quad w_3 = c^2 \left(\frac{ip}{\rho_0 \omega}\right)_z,
\tag{4.21}
$$

so that

$$
\nabla\left(\frac{ip}{\rho_0 \omega}\right) = -u_3 \hat{x} + \frac{w_3}{c^2} \hat{z}.
\tag{4.22}
$$

The unit vector along the slope is

$$
\hat{r} = \frac{\hat{x} + \alpha \hat{z}}{(1 + \alpha^2)^{1/2}},
\tag{4.23}
$$

and hence

$$
\nabla\left(\frac{ip}{\rho_0 \omega}\right) \cdot \hat{r} = -\frac{1}{(1 + \alpha^2)^{1/2}} \left(u_3 - \frac{\alpha}{c^2} w_3\right)
\tag{4.24}
$$

$$
= -\frac{1}{(1 + \alpha^2)^{1/2}} \cdot \frac{Q_c}{4h_s} \left[-\frac{(1 - \alpha/c)}{q} \right.
$$

$$
\left. \times V\left(1 - \frac{\eta}{2\gamma q}\right) - (1 + \alpha/c)V\left(-\frac{\xi}{2\gamma}\right) \right].
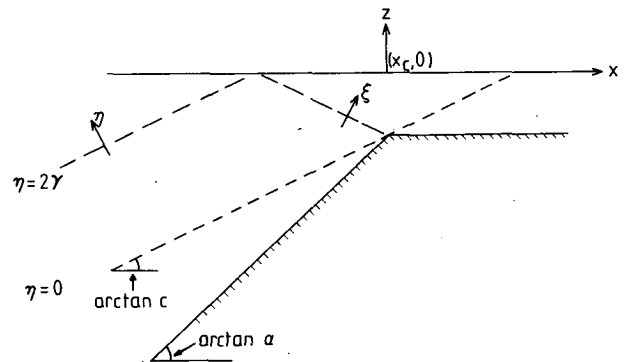\tag{4.25}
$$

On the slope we also have

FIG. 8. Definition sketch for flow of a stratified fluid with two-dimensional geometry.

$$1 - \frac{\eta}{2\gamma q} = -\frac{\xi}{2\gamma}, \qquad (4.26)$$

and substituting this into (4.25) shows that the bracketed term on the right hand side vanishes. Hence the pressure gradient along the surface of the continental slope is zero, regardless of the form of the function V. It follows that, for $\alpha/c > 1$, all the forcing of motion inside the narrow canyon is affected at the upper end on the shelf, since the pressure field is constant along the slope and is equal to the value at the shelf break. On the shelf the pressure field is barotropic so that $p = p_1$ as described in Section 3. The pressure field p_1 on the lower boundary for the solution shown in Fig. 6 is given in Fig. 9; on the part of the shelf corresponding to the position of the canyon the gradient dp_1/dx is constant, to a good approximation.

5. Baroclinic motion in the canyon

As stated above, we regard the total motion in the canyon as forced by the pressure field associated with the two-dimensional motion immediately outside it. This will be formally applicable in the limit of vanishing canyon width and it embodies the assumption that the canyon is sufficiently narrow to have a negligible effect on the exterior flow. However, before discussing motion in the canyon we must first consider the appropriate boundary condition at the open edges for the baroclinic motion inside it.
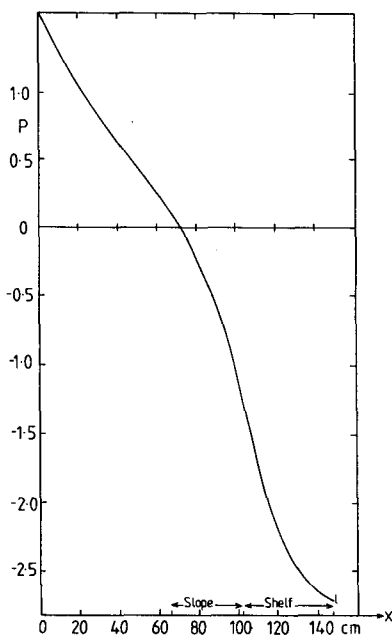

FIG. 9. The pressure field on the two-dimensional topographic surface (continental slope and shelf) for the solution shown in Fig. 6.

a. The open boundary condition

We consider the problem of reflection of a plane internal wave in a semi-infinite two-dimensional region of width 2a, from a plane where the fluid region opens abruptly into a semi-infinite half-space. The geometry is shown in Fig. 10. The problem is discussed in some detail and with greater generality by Grimshaw et al., (1982). This problem is an analogue of a classical wave–diffraction problem, and the relevant equations for this situation are summarized in Appendix C.

If we write the pressure field for the incident wave in the form

$$p_I = \exp[i(k(z - cx) - \omega t)]$$
$$= \exp\left[\frac{ik(1 + \alpha c)r}{(1 + \alpha^2)^{1/2}}\right] \exp[i(ms - \omega t)], \quad (5.1)$$

the primary reflected wave (with no y-dependence) from the junction $r = 0$ may be written

$$p_R = A'_0 \exp[i(k_R(z + cx) - \omega t)]$$
$$= A'_0 \exp\left[\frac{ik_R(1 - \alpha c)r}{(1 + \alpha^2)^{1/2}}\right] \exp[i(ms - \omega t)], \quad (5.2)$$

where

$$k_R = k \frac{\alpha - c}{\alpha + c}, \quad m = \frac{k(\alpha - c)}{(1 + \alpha^2)^{1/2}},$$

m being the along-slope wavenumber. The real part of these expressions is implied, and N and c are constants. The amplitude and phase of A'_0 are shown in Fig. 11, as a function of the gap width $2a$, for various values of α/c for $\alpha = 0.649$, the topographic slope in the experiment. Note that

$$A'_0 \rightarrow -1, \quad \text{as} \quad ma \rightarrow 0;$$

in this limit the appropriate boundary condition is

$$p = \text{constant},$$

and the reflected wave differs in phase by 180° from the corresponding wave that would be reflected from a rigid boundary. As $ma \rightarrow \infty$ the incident wave escapes completely into the open half-space. The situation is similar to that of the reflection of a sound wave from the open end of an organ pipe, although here the aperture is a slit rather than a circular orifice.

If k is altered in sign so that the wave–energy flux is reversed, i.e., the wave represented by (5.2) (with unit amplitude) is incident and that by (5.1) is reflected, then the amplitude of the reflected wave is A'_0 with the same value so that Fig. 11 applies to this case also. We may now discuss the nature of internal-wave modes in a narrow canyon, which are useful for interpretation of the observations.
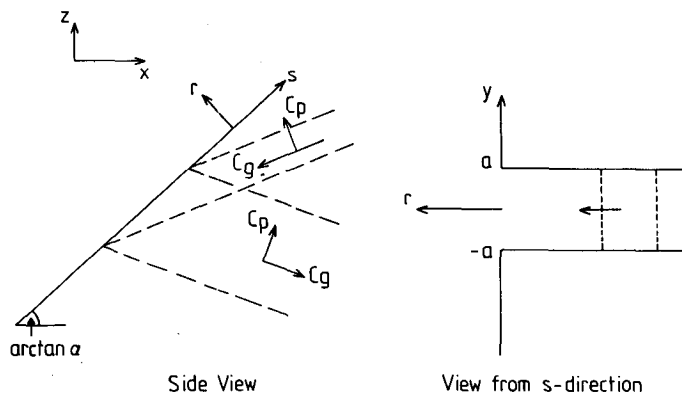
FIG. 10. Geometry for a plane internal wave propagating
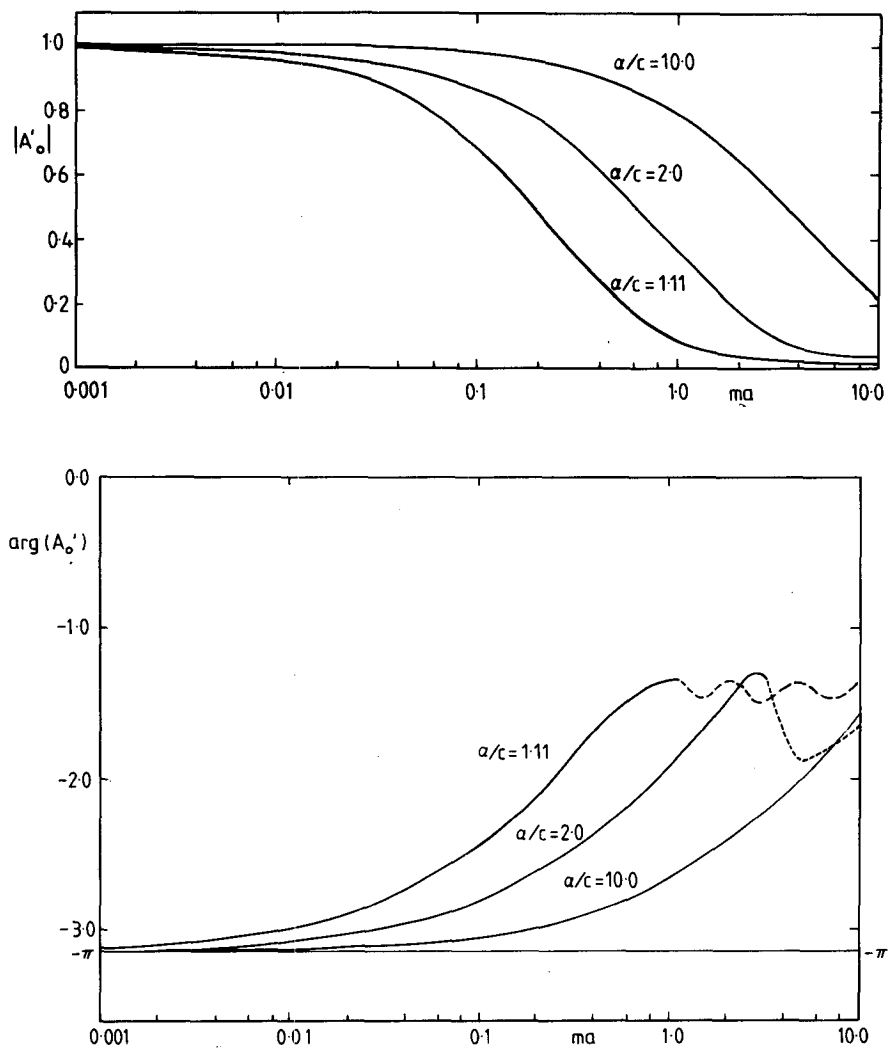in a vertical slit which opens into a half-space.

FIG. 11. Reflection coefficients for the streamfunctions for the plane wave of Fig. 10. A_0' is the relative
amplitude of the reflected wave with no cross-slit (y) variation. The curves have been computed for α
= 0.649, the value pertaining to the experiments.

b. Internal wave modes in a narrow canyon

We refer to Fig. 12 and define new coordinates x', z' and r, s which have their origin at the canyon head $(x = x_h, z = -h_s)$. The coordinate s is directed upslope with r normal to it, so that

$$r = \frac{z' - \alpha x'}{(1 + \alpha^2)^{1/2}}, \quad s = \frac{\alpha z' + x'}{(1 + \alpha^2)^{1/2}}, \quad (5.3)$$

and x', z', r, s all have the same units.

The equation for the total stream function ψ in terms of r and s is

$$(\alpha^2 - c^2)\psi_{rr} - 2\alpha(1 + c^2)\psi_{rs}$$
$$+ (1 - \alpha^2 c^2)\psi_{ss} = 0. \quad (5.4)$$

We look for normal modes of the form

$$\psi = \phi(r)e^{-ims}, \quad (5.5)$$

which satisfy

$$\psi = 0, \quad \text{on} \quad r = 0. \quad (5.6)$$

These have the form

$$\psi = (e^{im\beta_1 r} - e^{im\beta_2 r})e^{-ims}, \quad (5.7)$$

where

$$\beta_1 = -\frac{(1 - \alpha c)}{\alpha + c}, \quad \beta_2 = -\frac{1 + \alpha c}{\alpha - c}. \quad (5.8)$$

For a canyon with a perfectly reflecting open boundary, and horizontal breadth b, the boundary condition of constant pressure at

$$r = \frac{\alpha b}{(1 + \alpha^2)^{1/2}} = B \quad (5.9)$$

is

$$\psi_{z'} + \frac{\alpha}{c^2}\psi_{x'} = 0, \quad (5.10)$$

or

$$\left(1 - \frac{\alpha^2}{c^2}\right)\psi_r + \alpha\left(1 + \frac{1}{c^2}\right)\psi_s = 0. \quad (5.11)$$
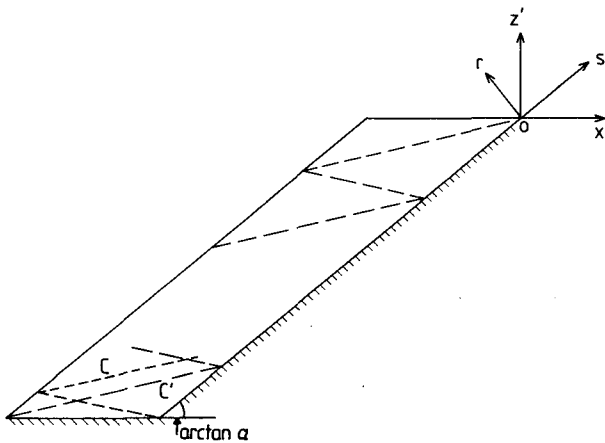

FIG. 12. Definition sketch for baroclinic motion in the canyon. Rays have been drawn for a typical case where $\alpha/c > 1$.

This condition gives eigenvalues for the wavenumber m, which are

$$m_n = \frac{\alpha^2 - c^2}{c(1 + \alpha^2)B}\frac{\pi}{2}(2n - 1),$$
$$n = 0, \pm 1, \pm 2, \cdots \quad (5.12)$$

We therefore have an infinity of modes which may be used to describe motion that is generated in a localized region of the canyon. The longest (lowest) mode has a length in the s-direction corresponding to two characteristic periods (as against one characteristic period for modes between two rigid boundaries at $r = 0$, B). For $\alpha/c < 1$ the directions of phase and energy propagation are the same for any given mode, whereas for $\alpha/c > 1$ the directions are opposite.

c. Leaky modes in a canyon of finite width

If the finite width of the canyon is considered so that the open boundary is only partially reflecting, the modal structure still has the form (5.7). We consider specifically the case $\alpha/c > 1$ with the wave–energy flux directed downward. Then the term in (5.7) containing β_2 denotes the η-wave, which is incident on the boundary $r = B$, whilst the β_1-term denotes the ξ-wave which emanates from $r = B$. Taking into account the reflection condition, we may write

$$e^{im\beta_1 B} = e^{i(\phi - \pi)} \cdot e^{im\beta_2 B}, \quad (5.13)$$

where we identify $e^{i(\phi - \pi)}$ with A_0' of Fig. 11, so that

$$|A_0'| = e^{-\phi_i}, \quad \arg A_0' = \phi_r - \pi, \quad (5.14)$$

where ϕ_r and ϕ_i denote the real and imaginary parts of ϕ. Hence the eigenvalues m_n are

$$m_n = \frac{\alpha^2 - c^2}{2c(1 + \alpha^2)B}(2n\pi + \phi_r - \pi + i\phi),$$
$$n = 0, -1, -2, \cdots \quad (5.15)$$

for downward energy flux. ϕ_r and ϕ_i may be determined from the curves of Fig. 11 by an iteration process, with

$$ma = \text{Re}(k_n a), \quad (5.16)$$

and starting with m_n given by (5.12) ($\phi = 0$). Note that the phase change ϕ_r accompanying partial reflection has the effect of reducing the effective wave number and hence increasing the amplitude of the reflection coefficient. These complex m_n result in a set of leaky modes which decay exponentially in amplitude as the energy propagates down the canyon (although in this case the phase propagates upward).

d. Application to forced flow in a canyon

We consider first the case $\alpha/c > 1$. As shown in Section 4, here the motion is forced at the line $z' = 0$. Over the range $-b < x' < 0$ the horizontal pres-

sure gradient is specified, implying that, inside the canyon,

$$\psi_{z'} = -f(x') \quad z' = 0, -b < x' < 0 \quad (5.17)$$

is specified. For canyons with a perfectly reflecting open boundary, if we ignore for the moment reflec-. tions from the bottom end, we may assume that the motion may be represented in the form

$$\psi = \sum_{n=0}^{-\infty} a_n e^{-im_n s}(e^{i\beta_1 m_n r} - e^{i\beta_2 m_n r}), \quad (5.18)$$

with the m_n given by (5.12). At $z' = 0$ equations 5.17 and 5.18 yield

$$\sum_{n=0}^{-\infty} (2n - 1)a_n g_n(x') = \frac{i2\alpha b}{\pi} f(x'),$$

$$-b < x' < 0, \quad (5.19)$$

where

$$g_n(x') = (\alpha/c + 1) \exp\left[i(2n - 1)(c/\alpha + 1)\frac{\pi x'}{2b} \right]$$

$$- (\alpha/c - 1) \exp\left[-i(2n - 1)(1 - c/\alpha)\frac{\pi x'}{b} \right]. \quad (5.20)$$

The functions $g_n(x')$ are not orthogonal. We may obtain the amplitudes a_n by multiplying (5.19) by g_m^* (the complex conjugate of g_m), integrating over $(-b, 0)$, and truncating the infinite set of linear equations obtained. Since

$$f(x') = \text{constant} = u_c, \quad (5.21)$$

from Fig. 9, the equations obtained have the form

$$\sum_{n=0}^{-\infty} G_{mn}(2n - 1)a_n = \frac{C}{2m - 1},$$

$$m = 0, -1, -2, \ldots, \quad (5.22)$$

where

$$C = \frac{4}{\pi^2} \frac{\alpha b u_c}{c(1 + \alpha^2/c^2)},$$

$$G_{mn} = 1, \quad m = n,$$

$$G_{mn} = \frac{\alpha/c}{[(\alpha/c)^2 + 1]\pi} \cdot \frac{\left[(2m - 1)(2n - 1)(-1)^{m+n} \sin\frac{\pi c}{\alpha}(n - m) - i\left\{ 2\left(1 - \frac{c^2}{\alpha^2} \right) \times (n - m)^2 + (2m - 1)(2n - 1)\left[1 - (-1)^{m+n} \cos\frac{\pi c}{\alpha}(n - m) \right] \right\} \right]}{(n - m)\left[(2m - 1)(2n - 1) + \left(1 - \frac{c^2}{\alpha^2} \right)(n - m)^2 \right]}, \quad m \neq n. \quad (5.23)$$

In practical situations the modes are leaky, and unless α/c is close to unity only the lowest modes penetrate to near the bottom of the canyon with significant amplitudes in the experiments. However, in general it is not appropriate to apply this procedure with the leaky modes to the boundary condition at $z = 0$, since the exponential decay, etc. only apply for $s < -b/(1 + \alpha^2)^{1/2}$. Hence we here adopt the procedure of using (5.19)–(5.23) to determine the initial amplitudes, and then regard the modes as leaky for $s < -b/(1 + \alpha^2)^{1/2}$.

For $\alpha/c < 1$ the situation is more complex because forcing by the external pressure field exists all along the outer boundary and also some energy may propagate toward the canyon head. However, the baroclinic motion is small for $\alpha/c \ll 1$ so that the flow is predominantly barotropic, and the concepts described above may be used to establish a qualitative interpretation of the flow for larger values of α/c.

6. Interpretation of observations

We now describe the observations in more detail in the light of the theoretical development of the preceding three sections. Photographic data was recorded for nine runs, as given in Table 1: five with the narrow canyon and four with the canyon mouth widened at

the foot (Fig. 2b). We will discuss these results in increasing order of α/c.

If $\alpha/c \ll 1$, computations for two-dimensional topography show that the generated baroclinic motion is small (Baines 1973). Hence we may expect this to be the case in the canyon situation also. Fig. 13 shows the characteristic pattern for $\alpha/c = 0.25$. The many reflections near the canyon head indicate that the local internal wavelength is much shorter than the scale of the barotropic forcing. Observations of the flow for

TABLE 1. Experimental parameters.

Run No.	α/c	Geometry	Piston amplitude a_p (cm)	Frequency ω (rad s⁻¹)
13	0.25	Narrow (Fig. 2a)	1.0	0.830
10	0.27	Narrow (Fig. 2a)	1.4	0.821
16	0.31	Wider at foot (Fig. 2b)	1.9	0.65
15	0.64	Wider at foot (Fig. 2b)	1.9	0.515
12	0.84	(Fig. 2a)	1.4	0.543
17	1.0	(Fig. 2b)	1.9	0.393
14	1.15	(Fig. 2a)	1.9	0.438
18	1.51	(Fig. 2b)	1.9	0.285
1A	1.69	(Fig. 2a)	2.4	0.319

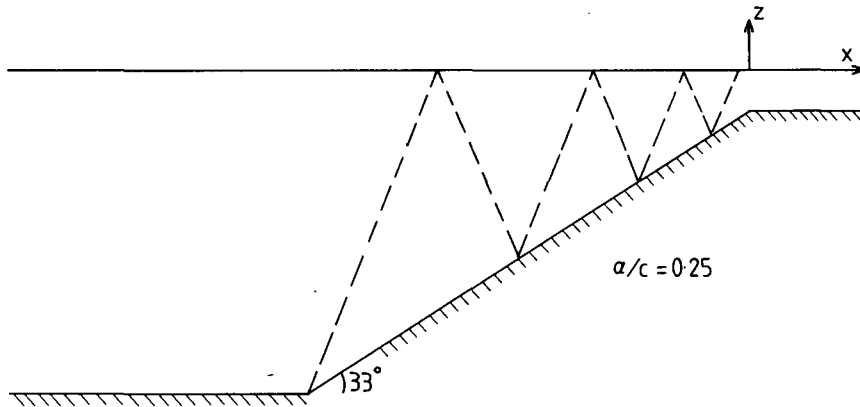For Run No. 1A the tank and shelf are longer than for the other runs.

FIG. 13. Typical rays for the internal waves for $\alpha/c = 0.25$.

$\alpha/c = 0.25$, 0.27 (narrow canyon—Runs 13, 10) and $\alpha/c = 0.31$ (wider canyon—Run 16) show motion which is totally in phase with the piston motion, and the flow pattern at the flood and ebb phases is qualitatively very similar to that of Fig. 7. The displacements of dye lines along the topography, both in the canyon and on the continental slope at the same depths, are shown in Fig. 14 as a function of time for $\alpha/c = 0.25$ (Run 13). The pattern follows that of the barotropic motion, with largest displacements occurring in the canyon near the canyon head. A qualitative comparison between the observed horizontal displacements on the canyon floor for the above three runs and the "barotropic" numerical solution is given in Fig. 15; the agreement is generally good, in spite of the scatter in the data. Hence, for $\alpha/c \lesssim 0.3$ at

least, the motion is almost entirely barotropic, with the largest motions occurring near the canyon head, and driven by the external pressure field.

As α/c increases toward unity, phase variations inside the canyon begin to become apparent and the region of significant motion extends farther down the canyon. Phase variations of up to quarter-period from the barotropic motion appear for $\alpha/c = 0.64$ and 0.84. These two flow patterns show significant differences, reflecting the fact that the flow depends on the characteristic geometry.

For $\alpha/c \geq 1$ the flow patterns in the canyon differ substantially from those for $\alpha/c < 1$ and also (for the runs of Table 1) from each other. For a perfectly reflecting open boundary, the model procedure of Section 5 converges increasingly slowly (i.e. more
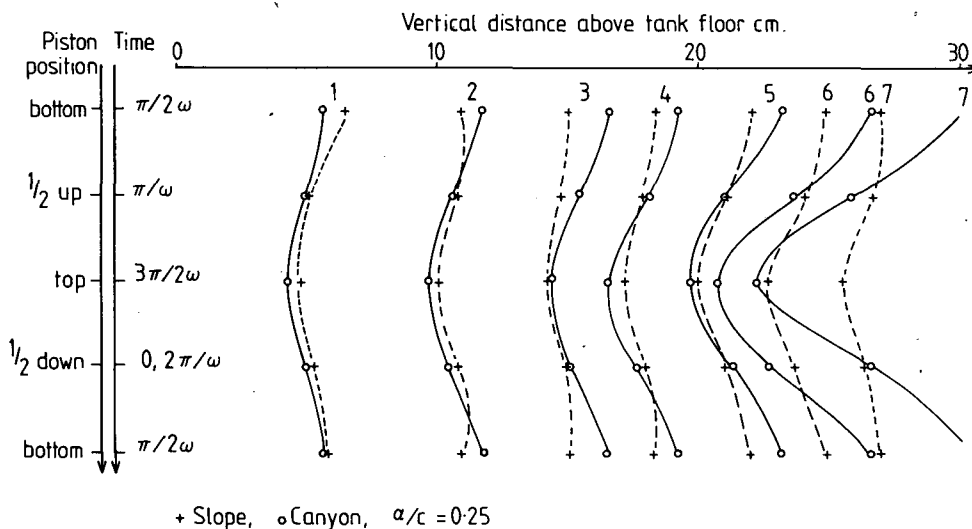

FIG. 14. Observed dye-line displacements as a function of time for $\alpha/c = 0.25$ (Run 13), measured on the continental slope (shown dashed) and on the canyon floor (solid). The circled numbers refer to the dye lines, numbered upward from the lowest.
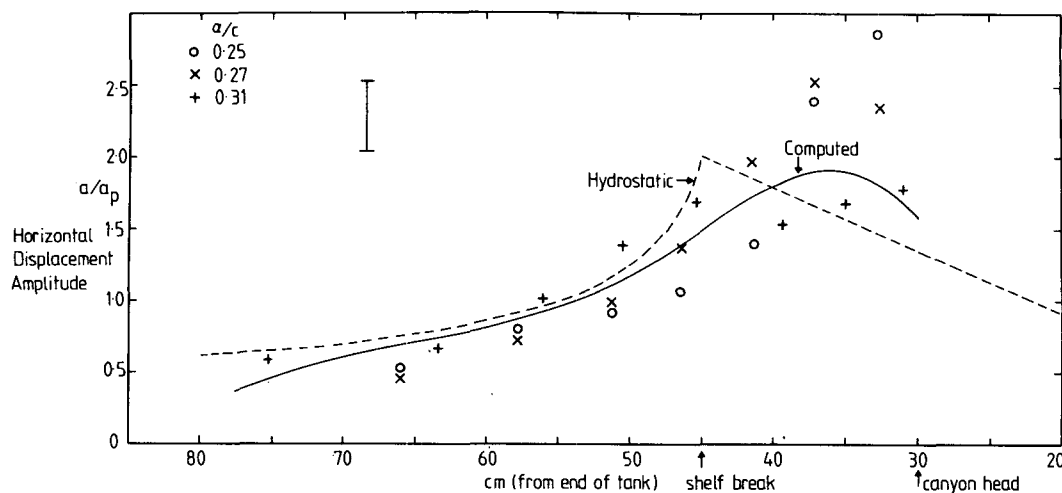
FIG. 15. Comparison between the observed horizontal displacement amplitudes on the canyon floor for Runs 13, 10 and 11, compared with the theoretical result from the solution of Fig. 7 (solid curve). The corresponding curve for hydrostatic flow is shown dashed.

modes are required) as $\alpha/c \rightarrow 1+$. The limit $\alpha/c = 1$ is singular, and the procedure is not applicable. Instead, one must resort to an integral equation approach, paralleling that used for two-dimensional topography (e.g., Baines, 1982). The details are too lengthy to warrant inclusion here, but the inviscid solution for $\alpha/c = 1$, assuming an infinite, bottomless canyon, is (to a good approximation)

$$\zeta_s = \frac{\bar{u}(1 + \alpha^2)^{1/2}}{2\omega} \left[\sin\omega t + \frac{1}{\pi} \left(\ln \left| \frac{b - (z'/c) + x'}{(z'/c) - x'} \right| \right. \right.$$
$$\left. \left. + \frac{b}{(z'/c) - x'} \right) \cos\omega t \right], \quad (6.1)$$

where ζ_s is the particle displacement parallel to the topography, and $\bar{u}$ is the mean barotropic velocity on the shelf over the canyon head. The flow patterns for $\alpha/c = 1$ (Run 11) are (at least) qualitatively consistent with (6.1), as may be seen from a comparison with Fig. 4. The pattern of motion of each dye line is the same, and they are (almost) in phase down the full length of the canyon. The phase propagation is outward, indicating downward energy flux, and there are large displacements near the canyon floor which probably reflect the presence of the inviscid singularity. The energy reaching the bottom cannot be reflected back inside the canyon, and it escapes through the canyon mouth after reflection from the tank bottom.

For $\alpha/c = 1.15$ (Run 14) the overall flow pattern is similar to that for $\alpha/c = 1.0$, in that the motion is almost the same down the full length of the canyon with an outward phase propagation; however, there are differences in detail—the displacements on the canyon floor, for example, are substantially different from those for $\alpha/c = 1$.

As α/c is increased further the character of the flow undergoes more significant changes. For $\alpha/c = 1.69$ (Run 11—the largest value studied) the motion is more complicated, with the largest amplitudes again occurring in the upper half of the canyon (vide Fig. 5); amplitudes measured on the canyon floor are shown in Fig. 16. The motion has the overall upward phase propagation and amplitude decreasing with depth expected from the theory of the previous section. The nature of the motion suggests nonlinear behavior. Similar behaviour (but different in detail) is observed for $\alpha/c = 1.51$ (Run 18). As described in the preceding sections, the motion in the canyon is forced by the time-varying pressure gradient on the shelf directly above the canyon. The resulting flow may be expressed as a set of modes which propagate energy down the canyon towards the foot. For $\alpha/c = 1.69$, the ratios of the streamfunction amplitudes of the lowest three modes, as determined from (5.23) are 1:0.185:0.086. Further, the decay rates due to leakage through the open boundary are such that only the lowest mode reaches the foot of the canyon with any significant amplitude; this is 71% of its amplitude at the canyon head. When this mode is "reflected" from the bottom of the tank it is scattered into the set of modes which propagate energy back up the canyon. The stream-function amplitudes of the lowest three such modes, again computed from (5.23), are in the ratio 1:0.35:0.54, with the amplitude of the lowest mode reduced by the factor of 0.44 in the reflection process. Of these upward energy-propagating (downward phase-propagating) modes, all but the lowest decay rapidly in the vertical.

The nature of the motion reflected from the bottom of the canyon may also be interpreted from the rays. For a perfectly reflecting open boundary the motion
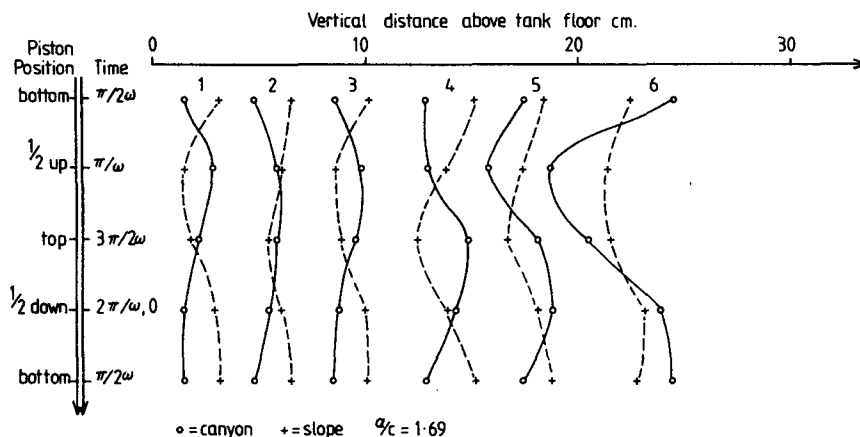
FIG. 16. As in Fig. 14 but for $\alpha/c = 1.69$ (Run 11).

near the corner ray (C' in Fig. 12) has the same phase as the incident motion, and therefore adds to it. Hence we expect larger motions here, particularly over the range CC'.

Overall, the motion in the canyon is fairly well described by the downward propagating first leaky mode, although the fit is not perfect, presumably because of the approximations involved and the presence of higher modes at both the top and bottom ends. The small-scale overturning visible near the bottom in Fig. 5 (Fig. 5a in particular, in the second-bottom dye layer) is probably due to the reflection of motion from the corner between the rays CC' of Fig. 12. In suitable circumstances this small-scale motion reflected from the corner may be quite significant.

7. Summary and discussion

The experiments designed here were originally designed for a first investigation of the nature of tidal flows in submarine canyons, and the rich range of phenomena observed was not expected. The observations made were not adequate for a definitive quantitative study in all cases, but provided an adequate qualitative picture which could be compared with a descriptive theoretical framework. There is scope for more detailed experiments of this type, covering the whole gamut of variable parameters.

The above experiments and theoretical discussion suggest that the nature of the tidal canyon motions may be grouped into five regimes, depending on the value of α/c. The boundaries of these regimes are not well defined and some may depend on factors not varied extensively in the experiments, such as canyon shape and amplitude of tidal forcing. The regimes are as follows.

1) $0 < \alpha/c \lesssim 0.4$. In this regime the stratification has very little effect on the flow, which is essentially

barotropic. The largest motions occur inside the canyon near the head.

2) $0.4 \lesssim \alpha/c < 1$. Here the motion is dominated by the barotropic motion, but also contains a baroclinic component which is sensitive to the ray geometry and has a down-canyon phase propagation.

3) $\alpha/c \approx 1$. Here the motion has virtually the same pattern at all depths down the canyon, with outward phase (downward energy) propagation. Energy loss by leakage through the open boundary is small until after reflection from the tank floor at the foot of the canyon; here most of the energy escapes directly through the open boundary.

4) $1 < \alpha/c \lesssim 10$. Here the wave energy of one or more modes propagates to the foot of the canyon where it is reflected into a number of upward-energy-propagating modes, most of which decay rapidly in the vertical. The superposition of these modes may result in large amplitude (and possibly strongly nonlinear) motions in the lower part of the canyon.

5) $\alpha/c \gg 1$. As α/c increases the wavenumber m_n increases, and hence from Fig. 11a the energy loss due to leakage also increases. Hence for α/c sufficiently large we have the situation where the modes generated at the canyon head do not reach the foot, so that the amplitude of the motion decays monotonically down the canyon. Unlike the situation where $\alpha/c \ll 1$, however, the motion is strongly baroclinic.

We conclude with some remarks about the relevance of these results for oceanic canyons. There are at least two significant aspects in which the experiment differs from oceanic conditions, namely that the experiment is not rotating, and that the topographic slope is much steeper in the tank than in the ocean. For narrow canyons, which are the main objects of the present study, the Coriolis force is expected to have a small effect on the motions inside the canyon
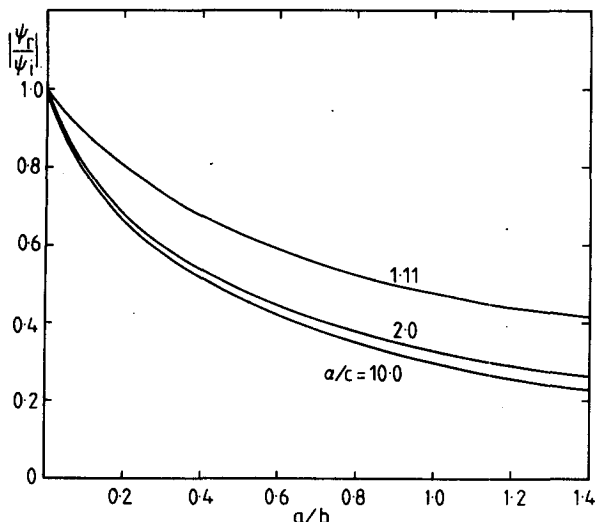
FIG. 17. Modulus of the reflection coefficients (for the stream function) for plane waves that correspond to the lowest internal mode propagating down the canyon, as a function of a/b where b is the horizontal breadth and a is the canyon half-width at the mouth. The figure has been computed for $\alpha = 0.1$, and is therefore representative of oceanic situations, although rotation is absent here.

per se, producing for the most part only a slight cross-canyon variation. The possible presence of internal Kelvin wave modes in not-so-narrow canyons introduces substantial complications which are currently being studied. Turning to the second point of small oceanic topographic slopes, computations using the equations of Appendix C for $\alpha \ll 1$ (specifically, $\alpha = 0.1$) show that the amplitude and phases of reflected waves as a function of ma are very similar to those presented in Fig. 11 for $\alpha = 0.649$. The importance of the internal reflection of internal waves from canyon mouths for oceanic geometries may be gauged from Fig. 17. This figure has been computed using the corresponding form of Fig. 11 for $\alpha = 0.1$, and gives the amplitude of the reflected stream function to that of the incident for the lowest mode, in a canyon with given ratio a/b, where a is the half-width at the mouth and b is the breadth. Since $a/b < 0.2$ for many canyons, these internal reflections will be significant.

Tidal motion in Hudson Canyon ($\alpha/c \approx 0.25$) is in regime 1, and this mechanism provides a plausible explanation for the tidal observations described by Hotchkiss and Wunsch (1982).

Finally, the above results have implications for internal waves that impinge on the mouth of a canyon from the outside (i.e. the deep sea). A sufficiently narrow canyon should have a negligible effect on the flow outside it so that internal waves impinging from the deep sea will reflect from a two-dimensional continental shelf with negligible perturbation. In partic-

ular the pressure field will be largely unchanged. However, if we consider the motion inside the canyon as forced by the external pressure field, this will be double that due to the original incident wave since it is the sum of the incident and reflected waves. Hence, in this narrow canyon limit, the incident wave will enter the canyon at double its external amplitude, and four times its external energy flux and density. This mechanism for the enhancement of internal wave energy in narrow canyons complements those proposed by Gordon and Marshall (1976) and Hotchkiss and Wunsch (1982) for wide-mouthed canyons, where the enhancement of wave energy may be due to narrowing geometry.

APPENDIX A

The Narrow Canyon Approximation

Here, we investigate the conditions under which it is possible to make the "narrow canyon" approximation, in which it is assumed that the motion in the canyon is driven by the externally imposed pressure outside it. We consider a simple model of hydrostatic wave motion in a channel of width B_1 with variable $h(y)$ across the channel. This system is a crude approximation to the flow situation of the experiment, but should give a good indication of the relative importance of the various parameters involved.

The equation for the free surface elevation ζ_0 is

$$\nabla^2 \zeta_{0_{tt}} = \nabla \cdot gh\nabla\zeta_0. \qquad (A1)$$

We assume that we have periodic waves propagating along the channel in the x-direction, i.e.

$$\zeta_0 = \zeta(y)e^{i(kx-\omega t)}, \qquad (A2)$$

where

$$\frac{d}{dy}\left(h\frac{d\zeta}{dy}\right) + \left(\frac{\omega^2}{g} - k^2h\right)\zeta = 0. \qquad (A3)$$

We take a cross-channel depth profile of the form

$$h(y) = \begin{cases} h_c, & 0 < y < b_1, \\ h_s, & b_1 < y < B_1, \end{cases} \qquad (A4)$$

with $h_s < h_c$ so that b_1 is the width of the deep region. The boundary conditions on $\zeta(y)$ are then

$$\zeta_y = 0, \qquad y = 0, B_1 \Big\}$$
$$h, \zeta_y \qquad y = b_1 \Big\} . \qquad (A5)$$
conditions

The solution is

$$\zeta = \begin{cases} \cos\alpha_c y/B_1, & 0 < y < b_1, \\ \cos\dfrac{\alpha_c b_1}{B_1} \cdot \dfrac{\cos\alpha_s(1 - y/B_1)}{\cos\alpha_s(1 - b/B_1)}, & b_1 < y < B_1, \end{cases} \qquad (A6)$$

where

$$\alpha_s^2 = \frac{\omega^2 B_1^2}{gh_s} - k^2 B_1^2, \quad \alpha_c^2 = \frac{\omega^2 B_1^2}{gh_c} - k^2 B_1^2, \quad (A7)$$

and k is given by

$$\alpha_s \tan\alpha_s(1 - b_1/B_1) = -h_c h_s^{-1}\alpha_c \tan\alpha_c b_1/B_1. \quad (A8)$$

For the canyon to have negligible effect on the free-surface elevation we require $|\alpha_c b_1/B_1| \ll 1$. Since $\alpha_s \rightarrow 0$ as $b_1 \rightarrow 0$, we must have $\alpha_c^2 < 0$ for sufficiently small b_1/B_1, from (A8). Then Eq. (A7) may be written

$$\left|\frac{\alpha_c b_1}{B_1}\right|^2 = \frac{\omega^2 b_1^2}{gh_s}(1 - h_s/h_c) - \left(\frac{\alpha_s b_1}{B_1}\right)^2, \quad (A9)$$

so that sufficient conditions for the neglect of the effect of the canyon on the free surface are

$$\frac{b_1}{B_1} \ll 1, \quad \frac{\omega^2 b_1^2}{gh_s} \ll 1. \qquad (A10)$$

APPENDIX B

Viscous Dissipation of Internal Waves Propagating Toward the Piston

For a monochromatic wave packet with wavenumber k and energy density E, the energy dissipation rate is $\nu k^2 E$, where ν is the kinematic viscosity. Hence we may write

$$E = E_0 e^{-\nu k^2 t}, \qquad (B1)$$

when E_0 is the energy density at $t = 0$. Since the packet travels with group velocity c_g we may write

$$r = c_g t, \quad E = E_0 \exp[-\nu k^2 r c_g^{-1}], \qquad (B2)$$

$$c_g = \frac{N}{|k|(1 + c^2)^{1/2}}. \qquad (B3)$$

With $k = 2\pi/L$ we therefore have

$$\frac{\nu|k^2|t}{c_g} = \frac{\nu}{N}\left(\frac{2\pi}{L}\right)^3 (1 + c^2)^{1/2} r. \qquad (B4)$$

If we take a representative value of L to be the width of the "beam" generated near the shelf break, we have, for the "worst" case in the experiments

(#11), $c = 0.38$, $N = 0.89$, $L = 6$ cm, $r = 300$ cm, $\nu = 0.01$ cm^2/s, so that

$$\exp(-\nu k^2 r c_g^{-1}) = e^{-3.6} = 0.03. \qquad (B5)$$

Hence viscous damping severely attenuates the baroclinic motions propagating toward the piston.

APPENDIX C

Equations Used For the Reflection/Diffraction of a Plane Internal Wave in a Slit Encountering a Half-Space

We consider the geometry shown in Fig. 10. For an incident wave of the form given by (5.1), i.e.,

$$p_I = \exp[i(k(z - cx)\omega t]$$
$$= \exp\left[\frac{ik(1 + \alpha c)r}{(1 + \alpha^2)^{1/2}}\right] \exp[i(ms - \omega t)], \quad (C1)$$

where $\qquad (C2)$

$$m = k(\alpha - c)/(1 + \alpha^2)^{1/2},$$

the backscattered wave in the slit may be expressed

$$p_s = \sum_{n=0}^{\infty} A_n' \cos(n\pi y/a)e^{ik_n' r}e^{i(ms - \omega t)}, \qquad (C3)$$

where

$$k_n'a = \left[\alpha(1 + c^2)ma - c(1 + \alpha^2)\right.$$
$$\left. \times \left\{(ma)^2 - n^2\pi^2 \frac{\alpha^2/c^2 - 1}{1 + \alpha^2}\right\}^{1/2}\right] \Big/ (\alpha^2 - c^2). \quad (C4)$$

If k_n' has a complex part, the appropriate sign gives a wave which decays exponentially away from the boundary. By use of the boundary conditions of continuity of pressure and normal velocity at the slit and the appropriate Green's function for the half-space, one obtains the following integral equation for the coefficients A_n' Grimshaw et al. (1982)

$$1 - i\gamma a \int_{-1}^{1} G(0, Y - S)dS = \sum_{n=0}^{\infty} A_n'\left\{-\cos n\pi Y\right.$$
$$\left. + i\beta_n a \int_{-1}^{1} G(0, Y - S) \cos n\pi S dS\right\}, \quad (C5)$$

where $Y = y/a$, $S = s/a$ and

$$G(0, Y - S) = -\frac{i}{2}\left(\frac{1 + \alpha^2}{\alpha^2 - c^2}\right)^{1/2} H_0^{(1)}(la|Y - S|), \quad (C6)$$

with

$$\left.\begin{aligned} \gamma a &= |m|ac \\ la &= |m|ac\left(\frac{1 + \alpha^2}{\alpha^2 - c^2}\right)^{1/2} \\ \beta_n a &= k_n'a \frac{\alpha^2 - c^2}{1 + \alpha^2} - ma\alpha \frac{1 + c^2}{1 + \alpha^2} \end{aligned}\right\} . \quad (C7)$$

Eq. (C5) has been solved numerically by use of a Galerkin technique to give the results for A_0' shown in Fig. 11.

REFERENCES

Baines, P. G., 1973: The generation of internal tides by flat-bump topography. *Deep Sea Res.*, **20**, 179–205.
——, 1974: The generation of internal tides over steep continental slopes. *Phil. Trans. Roy. Soc. London*, A277, 27–58.
——, 1982: On internal tide generation models. *Deep Sea Res.*, **29**, 307–338.
Gordon, R. L., and N. F. Marshall, 1976: Submarine canyons: internal wave traps? *Geophys. Res. Lett.*, **3**, 622–624.
Grimshaw, R. H. J., P. G. Baines and R. Bell, 1982: The reflection and diffraction of internal waves from the junction of a slit and a half-space, with application to submarine canyons. In preparation.
Hotchkiss, F. L., 1980: Internal gravity waves and sediment transport in Hudson submarine canyon. M.Sc. thesis, MIT, 116 pp.
——, and C. Wunsch, 1982: Internal waves in Hudson canyon with possible geological implications. *Deep Sea Res.*, **29**, 415–442.
Shepard, F. P., N. F. Marshall, P. A. McLoughlin and G. G. Sullivan, 1979: Currents in submarine canyons and other sea valleys. Amer. Assoc. Pet. Geol., Tulsa, 173 pp.
Wunsch, C., and S. Webb, 1979: The climatology of deep ocean internal waves. *J. Phys. Oceanogr.*, **9**, 235–243.